

Probing the nature of electroweak phase transition from particle colliders to gravitational wave detection

Fa Peng Huang¹, Youping Wan¹, Dong-Gang Wang², Yi-Fu Cai², and Xinmin Zhang¹

¹Theoretical Physics Division, Institute of High Energy Physics,
Chinese Academy of Sciences, P.O.Box 918-4, Beijing 100049, P.R.China and

²CAS Key Laboratory for Researches in Galaxies and Cosmology,
Department of Astronomy, University of Science and Technology of China,
Chinese Academy of Sciences, Hefei, Anhui 230026, China

In this letter, we explore the nature of the electroweak phase transition with both the particle colliders and the gravitational wave (GW) detection. With the observed Higgs mass, the shape of the Higgs potential is fully determined in the standard model of particle physics, however, it could be physically different. Working with the effective field theory, we will show the Higgs potential with a sextic term of the Higgs field included could give the 125 GeV Higgs mass, but a different Higgs potential. Furthermore, this Higgs scenario can produce a strong first order phase transition for the electroweak baryogenesis, and interestingly predict new physics in the Higgs sector, which can be tested at colliders such as the Large Hadron Collider (LHC) and the planning Circular Electron Positron Collider (CEPC). And we will also point out this strong first order phase transition will lead to a detectable GW signal for the GW interferometers, such as eLISA, DECIGO and BBO. Our study in this letter on the electroweak phase transition bridges the particle physics at colliders with the astrophysics and cosmology in the early universe.

PACS numbers: 04.30.-w, 12.60.-i, 95.55.-n

Introduction.— The central fundamental physics after the discovery of the Higgs boson [1, 2] is to explore the nature of the electroweak (EW) phase transition (PT) [3, 4]. This issue is closely related to the true shape of the Higgs potential. With the observed Higgs mass, the shape of the Higgs potential is fully determined in the standard model of particle physics, however, it could be physically different. In fact, the current data from colliders can only provide us with a very rough picture of these problems, and we know nothing but the quadratic oscillation around the vacuum expectation value (vev) v with the 125 GeV mass. For example, the true Higgs potential may be $V_{\text{tree}}(h) = \frac{1}{2}\mu^2 h^2 + \frac{\lambda}{4}h^4 + \frac{\kappa}{8\Lambda^2}h^6$, rather than the simplest case $V_{\text{tree}}(h) = \frac{1}{2}\mu^2 h^2 + \frac{\lambda}{4}h^4$ in the standard model (SM), as shown in Fig. 1.

Theoretically, this Higgs model with the sextic term has been shown to produce the strong first order PT

for EW baryogenesis [5–20]. In this paper we will study the new prediction of this model for collider physics and gravitational wave (GW) detection. Our results show that new physics associated with the modified trilinear Higgs coupling can be tested at the LHC and CEPC [21]. Furthermore, associated with the strong first order PT, large anisotropic fluctuations can be produced in the energy stress tensor and hence lead to unique patterns of GW spectra [22–25], which can be detected in the GW detectors, such as eLISA [26], DECIGO [27–29] and BBO [30].

The effective potential and Collider signals of PT— To investigate the EW PT, we begin with the following tree-level Higgs potential [14, 21]:

$$V_{\text{tree}}(h) = \frac{1}{2}\mu^2 h^2 + \frac{\lambda}{4}h^4 + \frac{\kappa}{8\Lambda^2}h^6. \quad (1)$$

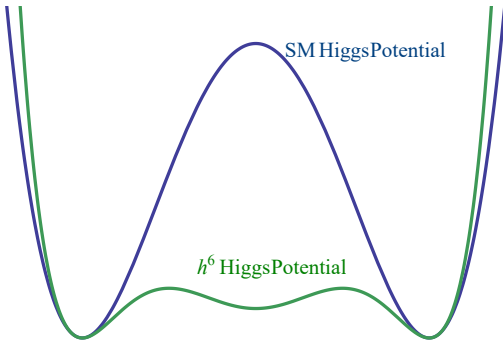


FIG. 1: Question of the nature of the Higgs potential and the EW PT.

Then, the finite-temperature effective potential up to one-loop level can be written as $V_{\text{eff}}(h, T) = V_{\text{tree}}(h) + V_1^{T=0}(h) + \Delta V_1^{T \neq 0}(h, T)$ [31], where $V_{\text{tree}}(h)$ is the potential at tree level, $V_1^{T=0}(h)$ is the one-loop Coleman-Weinberg potential at $T = 0$, and $\Delta V_1^{T \neq 0}(h)$ is the thermal contribution with the daisy resummation. In our case, the dominant contribution for the PT is from the tree-level barrier, and accordingly, the dominant effective potential with finite temperature effects is $V_{\text{eff}}(h, T)^{\text{dominant}} \approx \frac{\kappa}{8\Lambda^2}h^6 + \frac{\lambda}{4}h^4 + \frac{1}{2}(\mu^2 + cT^2)h^2$, with $c = \frac{1}{16}(-12\frac{\kappa v^2}{\Lambda^2} + g'^2 + 3g^2 + 4g_t^2 + 4\frac{m_h^2}{v^2})$. The completed one-loop effective potential is firstly given in Ref. [6].

¹ To fix the observed Higgs mass $m_h = 125$ GeV and the vev v , the model parameters λ and μ^2 are shifted to: $\lambda = \lambda_{\text{SM}}(1 - \frac{\Lambda_{\text{max}}^2}{\Lambda^2})$ and $\mu^2 = \mu_{\text{SM}}^2(1 - \frac{\Lambda_{\text{max}}^2}{2\Lambda^2})$, with $\Lambda_{\text{max}} \equiv \sqrt{3\kappa}v^2/m_h$.

Following the standard analysis of the EW PT/baryogenesis, the PT critical temperature T_c and the washout parameter $v(T_c)/T_c$ are approximated as follows,

$$T_c = \frac{\sqrt{\lambda^2\Lambda^2 - 4\kappa\mu^2}}{2\sqrt{c\kappa}}, \quad \frac{v(T_c)}{T_c} = \frac{2\Lambda\sqrt{-c\lambda}}{\sqrt{\lambda^2\Lambda^2 - 4\kappa\mu^2}}. \quad (2)$$

$T_c > 0$ gives a lower bound $\Lambda_{\text{min}} \equiv \Lambda_{\text{max}}/\sqrt{3} = \sqrt{\kappa}v^2/m_h$. For $m_h = 125$ GeV, one gets $\Lambda_{\text{min}} \approx 480\sqrt{\kappa}$ GeV. One also expects $\mu^2 + cT^2 > 0$ to stabilize the false vacuum, $\lambda < 0$ to produce a tree-level potential barrier, and then a positive h^6 term to stabilize the true vacuum. Consequently, the negative λ can yield an upper bound on Λ , namely, $\Lambda < \Lambda_{\text{max}} \approx 840\sqrt{\kappa}$ GeV. In addition, from the requirement of perturbativity, $\kappa < 4\pi$. If one chooses a larger κ , however, a larger bound Λ_{max} may be achieved. For $480 \text{ GeV} < \Lambda/\sqrt{\kappa} < 840 \text{ GeV}$, the washout factor $v(T_c)/T_c$ is larger than one, which means the strong first order PT can be achieved.

An interesting consequence is that the requirement of the strong first order PT can lead to an obvious modification of the trilinear Higgs boson coupling as $\mathcal{L}_{hhh} = -\frac{1}{6}(1 + \delta_h)A_h h^3$, with $A_h = 3m_h^2/v$ being the trilinear Higgs coupling in the SM and $\delta_h = 2\Lambda_{\text{min}}^2/\Lambda^2$ being in our scenario. In our theory δ_h varies from 2/3 to 2. Based on this properties, we can test this EW PT scenario by measuring the deviation of the trilinear Higgs coupling at the colliders. For the LHC, the deviation of the trilinear Higgs coupling leads different invariant mass distribution of the Higgs boson pair from the SM case. Due to the difficulties to suppress the large backgrounds at the hadron colliders, the trilinear Higgs coupling can not be completely pin down at the 14 TeV LHC. However, at the lepton collider, such as the International Linear Collider (ILC) and CEPC, the trilinear Higgs coupling can be measured precisely.

At the CEPC with $\sqrt{s} = 240$ GeV, the dominant one-loop contribution to hZ cross section (σ_{hZ}) beyond the SM is given by the modified trilinear Higgs coupling [21], which leads to the deviation of σ_{hZ} [21]. Such a deviation is defined as: $\delta_{\sigma_{hZ}} \equiv \sigma_{hZ}/\sigma_{hZ}^{\text{SM}} - 1$, which is approximately proportional to δ_h as $\delta_{\sigma_{hZ}} \simeq 1.6\%\delta_h$ at $\sqrt{s} = 240$ GeV. Thus, for $\kappa = 1$, one gets $\delta_{\sigma_{hZ}} \simeq \frac{7514.17 \text{ GeV}^2}{\Lambda^2}$. For the future CEPC with an integrated luminosity of 10 ab^{-1} , the precision of σ_{hZ} can be 0.4% [32], which corresponds

to $|\delta_h| \sim 25\%$ [21]. In our scenario, $\delta_h \in (2/3, 2)$, and hence, the associated signals are of observable interest at the CEPC.

GW signals of PT.— During the first order EW PT, there exists a potential barrier between the metastable vacuum and the false vacuum. If the PT is strong, true vacuum bubbles will be nucleated via quantum tunneling. The temperature goes down with the expanding of the universe, and the nucleation probability of one bubble per one horizon volume becomes larger and larger. The PT completes when the probability is of $\mathcal{O}(1)$ at the transition temperature, i.e. $\Gamma(T_*) \simeq H_*^4$, we obtain $S_3(T_*)/T_* = 4 \ln(T_*/100 \text{ GeV}) + 137$, in which $S_3 \equiv \int d^3r \left[\frac{1}{2}(\vec{\nabla}h)^2 + V_{\text{eff}}(h, T) \right]$ being the three dimensional Euclidean action.

The properties of the EW PT and the bubbles are determined two key PT parameters α and β . The parameter α is the ratio of the false-vacuum energy density $\epsilon(T)$ (the latent heat²) and the plasma thermal energy density $\rho_{\text{rad}}(T)$ ($\rho_{\text{rad}}(T) = \pi^2 g_*(T)T^4/30$) in the symmetric phase, which is defined by $\alpha \equiv \frac{\epsilon(T_*)}{\rho_{\text{rad}}(T_*)}$ at the transition temperature T_* . The other parameter β is defined as $\beta \equiv -\frac{dS_E}{dt} \Big|_{t=t_*} \simeq \frac{1}{\Gamma} \frac{d\Gamma}{dt} \Big|_{t=t_*}$, with $S_E(T) \simeq S_3(T)/T$ and $\Gamma = \Gamma_0(T) \exp[-S_E(T)]$ is the rate of variation of the bubble nucleation rate with $\Gamma_0(T) \propto T^4$. The parameter α gives a measure of the strength of the PT, the larger its value means a stronger PT has happened. While β^{-1} is the typical time scale of the PT, its product with the bubble wall velocity $\beta^{-1}v_b(\alpha)$ represents the size of the bubble wall.

The collisions of the Higgs bubbles and the turbulence of bubble with plasma are the two distinct mechanisms to generate the stochastic GW. The peak frequency produced by Higgs bubble collision is [33]

$$f_{\text{co}} \simeq 5.2 \times 10^{-6} \left(\frac{\beta}{H_*} \right) \left(\frac{T_*}{100 \text{ GeV}} \right) \left(\frac{g_*^t}{100} \right)^{1/6} \text{ Hz},$$

and the corresponding GW intensity is [33]

$$\Omega_{\text{co}}(f_{\text{co}})h^2 \simeq c\epsilon^2 \left(\frac{H_*}{\beta} \right)^2 \left(\frac{\alpha}{1 + \alpha} \right)^2 \left(\frac{v_b^3}{0.24 + v_b^3} \right) \left(\frac{100}{g_*^t} \right)^{\frac{1}{3}},$$

with $c = 1.1 \times 10^{-6}$. And, the parameter ϵ (which characterizes the fraction of latent heat that is transformed to fluid kinetic energy), the bubble velocity v_b and the turbulent fluid velocity $u_s(\alpha)$ are the functions of α [34]. Here, $g_*^t (= g_*(T_*))$ is the total number of effective degree of freedom at the transition temperature T_* . At low frequency the spectrum $\Omega_{\text{co}}(f)h^2$ increased as $f^{2.8}$, while at high frequency it decreased as f^{-1} [35].

¹ The coefficients g' and g are the $U(1)_Y$ and $SU(2)_L$ gauge couplings, and y_t is the top quark Yukawa coupling in the SM, respectively.

² where $\epsilon(T_{\text{tran}}) = [-V_{\text{eff}}^{\text{min}}(T) + T dV_{\text{eff}}^{\text{min}}/dT]_{T=T_{\text{tran}}}$.

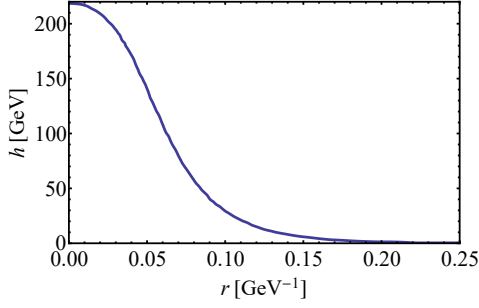


FIG. 2: The Higgs bubble profile for $\kappa = 1$, $T = 51.93564847$ GeV and $\Lambda = 600$ GeV.

On the other side, the GW signals produced by the turbulence interaction has a peak frequency at about [33]

$$f_{\text{tu}} \simeq 3.4 \times 10^{-6} \frac{u_s}{v_b} \left(\frac{\beta}{H_*} \right) \left(\frac{T_*}{100 \text{ GeV}} \right) \left(\frac{g_*^t}{100} \right)^{1/6} \text{ Hz},$$

with the intensity [33]

$$\Omega_{\text{tu}}(f_{\text{tu}}) h^2 \simeq 1.4 \times 10^{-4} u_s^5 v_b^2 \left(\frac{H_*}{\beta} \right)^2 \left(\frac{100}{g_*^t} \right)^{1/3}.$$

At low frequency the spectrum $\Omega_{\text{tu}}(f) h^2$ increased as f^2 , while at high frequency it decreased as $f^{-3.5}$ [33].

The two characteristic parameters α and β can be evaluated by solving the Higgs bubble profile from the following equation

$$\frac{d^2 h}{dr^2} + \frac{2}{r} \frac{dh}{dr} = \frac{\partial V_{\text{eff}}}{\partial h},$$

with the boundary conditions $h(r \rightarrow \infty) = 0$, $\frac{dh(r=0)}{dr} = 0$. Using the overshoot/undershoot method, the Higgs bubble profile can be obtained as shown in Fig. 2 for the case of $\kappa = 1$ and $\Lambda = 600$ GeV. For different Λ , the corresponding Higgs profiles can be obtained. When Λ becomes smaller than 590 GeV, the bubble wall runs away [36, 37]. Once the Higgs profile has been found, all the related parameters can be obtained, and the predicted GW spectra are shown in Fig. 3.

Combined Results and Discussions.— In Fig. 3, the GW spectra $h^2 \Omega_{\text{GW}}$ and the hZ cross section deviations $\delta_{\sigma_{hZ}}$ are shown for different cutoff scales Λ (590 GeV, 600 GeV, 650 GeV and 700 GeV) with $\kappa = 1$ in this scenario. The red line depicts the predicted GW signal for $\Lambda = 590$ GeV, which also corresponds to the prediction of $\delta_{\sigma_{hZ}} \simeq 2.2\%$ at the CEPC. The blue, green and black lines are the cases for 600 GeV, 650 GeV and 700 GeV, respectively, which indicates that the strength of GW is more significant for small cutoff scales. This fact can be naturally explained by the observation that in Eq.(1) a smaller Λ yields a larger contribution of the dimension-6 operators which enforce stronger EW PT. Meanwhile, it is found that the signals of GW are peaked around 10^{-4} Hz,

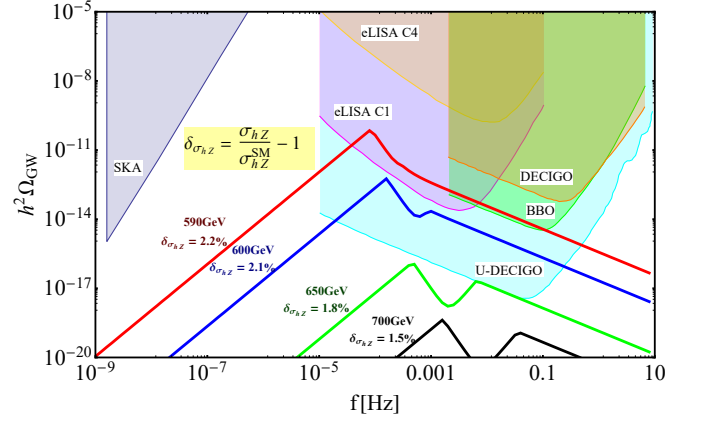


FIG. 3: GW spectra $h^2 \Omega_{\text{GW}}$ and the hZ cross section deviations $\delta_{\sigma_{hZ}}$ for different cutoff scales Λ (590 GeV, 600 GeV, 650 GeV and 700 GeV) with $\kappa = 1$ in this scenario. The above colored regions show the expected experimental sensitivities at future GW interferometers for eLISA, DECIGO, BBO, U-DECIGO and SKA, respectively. The red line depicts the GW signal for $\Lambda = 590$ GeV, which also gives rise to a signal of $\delta_{\sigma_{hZ}} \simeq 2.2\%$ at the CEPC. The blue, green and black lines are the cases for 600 GeV, 650 GeV and 700 GeV, respectively.

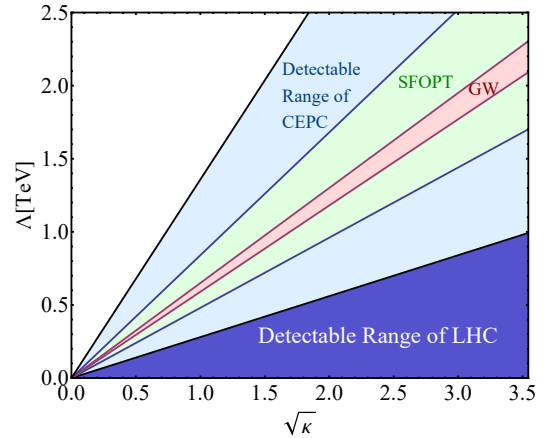


FIG. 4: The observational abilities of different experiments. For CEPC, the sensitive region is $\Lambda/\sqrt{\kappa} < 1357.65$ GeV; for LHC, it corresponds to $\Lambda/\sqrt{\kappa} < 280$ GeV; the theoretical condition for the strong first order PT requires $480 \text{ GeV} < \Lambda/\sqrt{\kappa} < 840 \text{ GeV}$; and the detectable region of GW interferometers reads $590 \text{ GeV} < \Lambda/\sqrt{\kappa} < 700 \text{ GeV}$.

which lies in the detectable range of satellite based GW experiments. The above colored regions show the expected experimental sensitivities at future GW interferometers including eLISA³ [38], SKA, BBO, DECIGO [39] and

³ eLISA C1 and C4 in Fig. 3 are two representative configurations studied in Ref.[38]

Ultimate-DECIGO (U-DECIGO) [40]. As shown in Fig. 3, eLISA, BBO and U-DECIGO are all capable of detecting the GW generated during the EW PT in our scenario.

Therefore, the collider experiments in particle physics and the GW experiments are naturally related to each other during the exploring the nature of the EW PT, i.e. there is a strong correlation between the strength of the GWs and the deviation of the trilinear Higgs coupling. As shown in Fig. 3, each lines relates the GW signals and the corresponding collider signals with the same cutoff energy scale.

In Fig. 4, the observational abilities of different experiments are shown. For CEPC with $\sqrt{s} = 240$ GeV, the sensitive region is $\Lambda/\sqrt{\kappa} < 1357.65$ GeV; for LHC, it corresponds to $\Lambda/\sqrt{\kappa} < 280$ GeV; the theoretical condition for the strong first order PT roughly requires $480 \text{ GeV} < \Lambda/\sqrt{\kappa} < 840$ GeV; and the detectable region of GW interferometers reads $590 \text{ GeV} < \Lambda/\sqrt{\kappa} < 700$ GeV. For the probing of the EW PT/baryogenesis, the detectable ability of the LHC is weak, but the future CEPC and the GW detections just have the ability to precisely detect the predicted signals. The GW observation experiments in space can provide a complementary approach to explore the nature of the EW PT beyond terrestrial colliders, and vice versa.

Conclusion— After the discovery of the 125 GeV Higgs boson, it becomes a urgent problem to unravel the nature of the EW PT. If the EW PT is strong first order, it will naturally relate to the mechanism of the spontaneous symmetry breaking, the EW baryogenesis and the PT GW. We have studied the EW PT in the frame work of EFT and investigated how to test this scenario at colliders. The complementary approach has also been discussed in this letter by considering the PT GW, and we have found that the GW produced by the bubble collision and turbulence with the plasma during the first order PT was just within the future GW experimental precision. These study will helps us to understand the nature of the EW PT, open a new window into the particle physics, and highlights the collection between the particle physics and cosmology.

Acknowledgements.— FPH, YPW and XZ are supported in part by the NSFC under grants Nos. 11121092, 11033005, 11375220 and also by the CAS pilotB program. DGW and YFC are supported in part by the Chinese National Youth Thousand Talents Program and by the USTC start-up funding under Grant No. KY2030000049. The operation of this super-computation is funded by the particle cosmology group at USTC.

[1] G. Aad *et al.* [ATLAS Collaboration], Phys. Lett. B **716**, 1 (2012) [arXiv:1207.7214 [hep-ex]].

[2] S. Chatrchyan *et al.* [CMS Collaboration], Phys. Lett. B **716**, 30 (2012) [arXiv:1207.7235 [hep-ex]].

[3] CEPC-SPPC Study Group, IHEP-CEPC-DR-2015-01, IHEP-TH-2015-01, HEP-EP-2015-01.

[4] N. Arkani-Hamed, T. Han, M. Mangano and L. T. Wang, arXiv:1511.06495 [hep-ph].

[5] C. Grojean and G. Servant, Phys. Rev. D **75**, 043507 (2007) [hep-ph/0607107].

[6] C. Delaunay, C. Grojean and J. D. Wells, JHEP **0804**, 029 (2008) [arXiv:0711.2511 [hep-ph]].

[7] S. J. Huber and T. Konstandin, JCAP **0805**, 017 (2008) [arXiv:0709.2091 [hep-ph]].

[8] S. Das, P. J. Fox, A. Kumar and N. Weiner, JHEP **1011**, 108 (2010) [arXiv:0910.1262 [hep-ph]].

[9] J. R. Espinosa, T. Konstandin, J. M. No and M. Quiros, Phys. Rev. D **78**, 123528 (2008) [arXiv:0809.3215 [hep-ph]].

[10] M. Jarvinen, C. Kouvaris and F. Sannino, Phys. Rev. D **81**, 064027 (2010) [arXiv:0911.4096 [hep-ph]].

[11] J. R. Espinosa, T. Konstandin, J. M. No and G. Servant, JCAP **1006**, 028 (2010) [arXiv:1004.4187 [hep-ph]].

[12] P. Schwaller, Phys. Rev. Lett. **115**, 181101 (2015) [arXiv:1504.07263 [hep-ph]].

[13] M. Kakizaki, S. Kanemura and T. Matsui, Phys. Rev. D **92**, 115007 (2015) [arXiv:1509.08394 [hep-ph]].

[14] X. m. Zhang, Phys. Rev. D **47**, 3065 (1993) [hep-ph/9301277].

[15] X. Zhang and B. L. Young, Phys. Rev. D **49**, 563 (1994) [hep-ph/9309269].

[16] X. Zhang, B. L. Young and S. K. Lee, Phys. Rev. D **51**, 5327 (1995) [hep-ph/9406322].

[17] X. Zhang, S. K. Lee, K. Whisnant and B. L. Young, Phys. Rev. D **50**, 7042 (1994) [hep-ph/9407259].

[18] K. Whisnant, B. L. Young and X. Zhang, Phys. Rev. D **52**, 3115 (1995) [hep-ph/9410369].

[19] B. Grzadkowski, J. Pliszka and J. Wudka, Phys. Rev. D **69**, 033001 (2004) [hep-ph/0307338].

[20] F. P. Huang and C. S. Li, Phys. Rev. D **92**, 075014 (2015) [arXiv:1507.08168 [hep-ph]].

[21] F. P. Huang, P. H. Gu, P. F. Yin, Z. H. Yu and X. Zhang, arXiv:1511.03969 [hep-ph].

[22] E. Witten, Phys. Rev. D **30**, 272 (1984).

[23] C. J. Hogan, Phys. Lett. B **133**, 172 (1983).

[24] C. J. Hogan, Mon. Not. Roy. Astron. Soc. **218**, 629 (1986).

[25] M. S. Turner and F. Wilczek, Phys. Rev. Lett. **65**, 3080 (1990).

[26] P. A. Seoane *et al.* [eLISA Collaboration], arXiv:1305.5720 [astro-ph.CO].

[27] N. Seto, S. Kawamura and T. Nakamura, Phys. Rev. Lett. **87**, 221103 (2001) [astro-ph/0108011].

[28] S. Kawamura *et al.*, Class. Quant. Grav. **23**, S125 (2006). doi:10.1088/0264-9381/23/8/S17

[29] S. Kawamura *et al.*, Class. Quant. Grav. **28**, 094011 (2011). doi:10.1088/0264-9381/28/9/094011

[30] V. Corbin and N. J. Cornish, Class. Quant. Grav. **23**, 2435 (2006) [gr-qc/0512039].

[31] M. Quiros, hep-ph/9901312.

[32] M. Bicer *et al.* [TLEP Design Study Working Group Collaboration], JHEP **1401**, 164 (2014) [arXiv:1308.6176 [hep-ex]].

[33] A. Nicolis, Class. Quant. Grav. **21**, L27 (2004) [gr-qc/0303084].

[34] M. Kamionkowski, A. Kosowsky and M. S. Turner, Phys. Rev. D **49**, 2837 (1994) [astro-ph/9310044].

- [35] S. J. Huber and T. Konstandin, JCAP **0809**, 022 (2008) [arXiv:0806.1828 [hep-ph]].
- [36] D. Bodeker and G. D. Moore, JCAP **0905**, 009 (2009) [arXiv:0903.4099 [hep-ph]].
- [37] S. J. Huber and M. Sopena, arXiv:1302.1044 [hep-ph].
- [38] C. Caprini *et al.*, arXiv:1512.06239 [astro-ph.CO].
- [39] C. J. Moore, R. H. Cole and C. P. L. Berry, Class. Quant. Grav. **32**, no. 1, 015014 (2015) doi:10.1088/0264-9381/32/1/015014 [arXiv:1408.0740 [gr-qc]].
- [40] H. Kudoh, A. Taruya, T. Hiramatsu and Y. Himemoto, Phys. Rev. D **73**, 064006 (2006) [gr-qc/0511145].